arXiv:1604.07050v1 [cond-mat.mtrl-sci] 24 Apr 2016

Ab initio computational study on the lattice thermal conductivity of Zintl clathrates $[Si_{19}P_4]Cl_4$ and $Na_4[Al_4Si_{19}]$

Ville J. Härkönen*
Department of Chemistry, University of Jyväskylä, PO Box 35, FI-40014, Finland

Antti J. Karttunen†
Department of Chemistry, Aalto University, FI-00076 Espoo, Finland.

(Dated: April 26, 2016)

The lattice thermal conductivity of silicon clathrate framework Si_{23} and two Zintl clathrates, $[Si_{19}P_4]Cl_4$ and $Na_4[Al_4Si_{19}]$, is investigated by using an iterative solution of the linearized Boltzmann transport equation (BTE) in conjuntion with *ab initio* lattice dynamical techniques. At 300 K, the lattice thermal conductivities for Si_{23}, $[Si_{19}P_4]Cl_4$, and $Na_4[Al_4Si_{19}]$ were found to be 43 W/(m K), 25 W/(m K), and 2 W/(m K), respectively. In the case of $Na_4[Al_4Si_{19}]$, the order-of-magnitude reduction in the lattice thermal conductivity was found to be mostly due to relaxation times and group velocities differing from Si_{23} and $[Si_{19}P_4]Cl_4$. The difference in the relaxation times and group velocities arises primarily due to the phonon spectrum at low frequencies, resulting eventually from the differences in the second-order interatomic force constants (IFCs). The obtained third-order IFCs were rather similar for all materials considered here.

I. INTRODUCTION

The minimization of the lattice thermal conductivity is usually a desired feature when higher thermoelectric efficiency is pursued[1,2]. There are several different classes of materials that appear to be promising for the thermoelectric applications, one example of such materials being the Zintl clathrates, also known as semiconducting clathrates[3–8]. The lattice thermal conductivity of the Zintl clathrates has been studied rather intensively in the past two decades[9–30] and several mechanisms have been proposed to explain the reduced lattice thermal conductivity values in these materials. In particular, lattice thermal conductivity values as low as $\sim$ 1 W/m K at 150 K have been obtained experimentally for some silicon clathrates[7,16] (single crystal samples). Recent experimental and computational studies have given rise to different points of view for the reasons behind the reduction of the lattice thermal conductivity in various clathrates[25,27]. In Ref.[25] it was concluded that the reduction of the lattice thermal conductivity of the Ba_8Si_{46} clathrate is mostly due to the harmonic phonon spectrum, while in Ref.[27] for the clathrate $Ba_8Ga_{16}Ge_{30}$ the reduction was suggested to arise mainly from rather short relaxation times (RTs). This work brings further perspectives on these issues by using computational techniques applied on two different types of Zintl clathrates.

In this work, we study the lattice thermal conductivity of the silicon clathrate framework Si_{23} (sometimes denoted as VIII or Si_{46}-VIII) and two hypothetical Zintl clathrate structures $[Si_{19}P_4]Cl_4$ and $Na_4[Al_4Si_{19}]$, obtained by adding guest atoms and framework heteroatoms in the Si_{23} structure. All the considered structures possess the same space group symmetry, which facilitates the comparative analysis of these materials since some quantities for the materials are identical. The study is carried out by using the Boltzmann transport equation (BTE) approach implemented in the open source program package ShengBTE. The harmonic phonon eigenvalues and eigenvectors used in the lattice thermal conductivity calculations are obtained by using density functional perturbation theory as implemented in the Quantum Espresso (QE) program package. In particular, the third-order interatomic force constants (IFCs) and quantities within the harmonic approximation are analyzed in order to understand their role in the reduction of lattice thermal conductivity. The results indicate that in the studied structures, the increased anharmonicity can be mostly explained by harmonic quantities and rather low lattice thermal conductivity values do not necessarily indicate exceptionally strong third-order IFCs.

II. THEORY, COMPUTATIONAL METHODS AND STUDIED STRUCTURES

A. Lattice dynamics

The theory of lattice dynamics discussed in this section has been considered, for instance, in Refs.[31–33]. The notation used here is the same as in Ref.[34]. In the present approach, one assumes that the lattice Hamiltonian is of the form

$$\hat{H} = \hat{H}_0 + \hat{H}_A, \tag{1}$$

where the harmonic Hamiltonian operator $\hat{H}_0$ may be written as

$$\hat{H}_0 = \sum_{\lambda} \hbar\omega_\lambda \left(\frac{1}{2} + \hat{a}^\dagger_\lambda \hat{a}_\lambda\right), \quad \lambda \equiv \mathbf{q}j, \tag{2}$$

and the anharmonic Hamiltonian operator $\hat{H}_A$ can be written as

$$\hat{H}_A = \sum_{\lambda} V(\lambda)\, \hat{A}_\lambda + \sum_{n=3} \sum_{\lambda_1} \cdots \sum_{\lambda_n} \times V(\lambda_1; \ldots; \lambda_n)\, \hat{A}_{\lambda_1} \cdots \hat{A}_{\lambda_n}, \quad \lambda_i \equiv \mathbf{q}_i j_i. \tag{3}$$

In Eq. 3

$$\hat{A}_\lambda = \hat{a}_\lambda + \hat{a}^\dagger_{-\lambda}, \quad -\lambda \equiv -\mathbf{q}j, \tag{4}$$

and[31]

$$\begin{aligned} &V(\lambda_1;\ldots;\lambda_n) \\ &= \frac{1}{n!N^n}\left(\frac{\hbar}{2}\right)^{n/2}\frac{\Delta\left(\mathbf{q}_1+\cdots+\mathbf{q}_n\right)}{\left[\omega_{\lambda_1}\cdots\omega_{\lambda_n}\right]^{1/2}} \\ &\times \sum_{\kappa_1,\alpha_1}\sum_{l_2,\kappa_2,\alpha_2}\cdots\sum_{l_n,\kappa_n,\alpha_n}\Phi_{\alpha_1\cdots\alpha_n}\left(0\kappa_1;l_2\kappa_2;\ldots;l'_n\kappa'_n\right) \\ &\times\frac{e_{\alpha_1}\left(\kappa_1|\lambda_1\right)}{M_{\kappa_1}^{1/2}}\cdots\frac{e_{\alpha_n}\left(\kappa_n|\lambda_n\right)}{M_{\kappa_n}^{1/2}}e^{i[\mathbf{q}_2\cdot\mathbf{x}(l_2)+\cdots+\mathbf{q}_n\cdot\mathbf{x}(l_n)]}. \end{aligned} \tag{5}$$

In Eq. 5

$$\begin{aligned} &\Phi_{\alpha_1\cdots\alpha_n}\left(l_1\kappa_1;\ldots;l_n\kappa_n\right) \\ &\equiv \left.\frac{\partial^n\Phi}{\partial x'_{\alpha_1}\left(l_1\kappa_1\right)\cdots\partial x'_{\alpha_n}\left(l_n\kappa_n\right)}\right|_{\{x'(l_i\kappa_i)=x(l_i\kappa_i)\}}, \end{aligned} \tag{6}$$

are the so-called nth order atomic force constants or interatomic force constants (IFCs), which are derivatives of the potential energy Φ, $\{\alpha_i\}$ are Cartesian indices, $\{\mathbf{q}_i\}$ phonon wave vectors (the wave vector times 2π), $\{j_i\}$ phonon mode indices, $\{\mathbf{e}\left(\kappa_i|\lambda_i\right)\}$ phonon eigenvectors, $\{\omega_{\lambda_i}\}$ phonon eigenvalues, $\{M_{\kappa_i}\}$ atomic masses of atoms $\{\kappa_i\}$ and $\mathbf{x}\left(l\kappa\right)=\mathbf{x}\left(l\right)+\mathbf{x}\left(\kappa\right)$, where $\mathbf{x}\left(l\right)$ is the lattice translational vector and $\mathbf{x}\left(\kappa\right)$ the position vector of atom κ within the unit cell. Furthermore, $\hat{a}^\dagger_\lambda$ and $\hat{a}_\lambda$ are the so-called creation and annihilation operators for phonons, respectively.

The diagonalization of the Hamiltonian was obtained with the following expansions for displacement and momentum

$$\hat{u}_\alpha\left(l\kappa\right)=\left(\frac{\hbar}{2N^2M_\kappa}\right)^{1/2}\sum_\lambda\omega_\lambda^{-1/2}e^{i\mathbf{q}\cdot\mathbf{x}(l)}e_\alpha\left(\kappa|\lambda\right)\hat{A}_\lambda, \tag{7}$$

$$\hat{p}_\alpha\left(l\kappa\right)=-i\left(\frac{\hbar M_\kappa}{2N^2}\right)^{1/2}\sum_\lambda\omega_\lambda^{1/2}e^{i\mathbf{q}\cdot\mathbf{x}(l)}e_\alpha\left(\kappa|\lambda\right)\hat{B}_\lambda, \tag{8}$$

where N is the number of $\mathbf{q}$-points in the $\mathbf{q}$-mesh and

$$\hat{B}_\lambda=\hat{a}_\lambda-\hat{a}^\dagger_{-\lambda}. \tag{9}$$

The phonon eigenvectors and eigenvalues can be obtained from the eigenvalue equation

$$\omega_j^2\left(\mathbf{q}\right)e_\alpha\left(\kappa|\mathbf{q}j\right)=\sum_{\kappa',\beta}D_{\alpha\beta}\left(\kappa\kappa'|\mathbf{q}\right)e_\beta\left(\kappa'|\mathbf{q}j\right), \tag{10}$$

with

$$D_{\alpha\beta}\left(\kappa\kappa'|\mathbf{q}\right)\equiv\sum_l\frac{\Phi_{\alpha\beta}\left(l\kappa;0\kappa'\right)}{\sqrt{M_\kappa M_{\kappa'}}}e^{-i\mathbf{q}\cdot\mathbf{x}(l)}. \tag{11}$$

The components of the eigenvector $\mathbf{e}\left(\kappa|\mathbf{q}j\right)$ are usually chosen to satisfy the following orthonormality and closure conditions

$$\sum_{\kappa,\alpha}e_\alpha\left(\kappa|\mathbf{q}j'\right)e^*_\alpha\left(\kappa|\mathbf{q}j\right)=\delta_{jj'}, \tag{12}$$

$$\sum_j e_\alpha\left(\kappa|\mathbf{q}j\right)e^*_\beta\left(\kappa'|\mathbf{q}j\right)=\delta_{\alpha\beta}\delta_{\kappa\kappa'}, \tag{13}$$

where $\delta_{\alpha\beta}$ is the Kronecker delta. One may interpret $\mathbf{e}\left(\kappa|\mathbf{q}j\right)e^{i\mathbf{q}\cdot\mathbf{x}(l)}$ as the probability amplitude and

$$\left|\mathbf{e}\left(\kappa|\mathbf{q}j\right)e^{i\mathbf{q}\cdot\mathbf{x}(l)}\right|^2=\left|\mathbf{e}\left(\kappa|\mathbf{q}j\right)\right|^2, \tag{14}$$

as the probability that the atom $l\kappa$ vibrates in the phonon mode $\mathbf{q}j$[35].

B. Thermal conductivity

By using the BTE approach[36,37], one may write for the lattice thermal conductivity[38–41]

$$\kappa_{\alpha\beta}=\frac{\hbar}{k_BTV}\sum_\lambda\omega_\lambda v_\alpha\left(\lambda\right)\bar{n}_\lambda\left(\bar{n}_\lambda+1\right)F_{\beta,\lambda}, \tag{15}$$

where V is the volume of the unit cell, k_B is the Boltzmann constant, $\mathbf{v}\left(\lambda\right)$ is the phonon group velocity and $\bar{n}_\lambda$ the equilibrium distribution function for the state λ. The unknown term $F_{\beta,\lambda}$ is obtained by solving the iterative equation

$$\begin{aligned} F_{\alpha,\lambda}=&\frac{1}{X_\lambda}\sum_{\lambda'}\sum_{\lambda''}\left[\Gamma^{\lambda''}_{\lambda\lambda'}\left(F_{\alpha,\lambda''}-F_{\alpha,\lambda'}\right)\right. \\ &\left.+\Gamma^{\lambda'\lambda''}_{\lambda}\left(F_{\alpha,\lambda'}+F_{\alpha,\lambda''}\right)\right] \\ &+\frac{\hbar\omega_\lambda v_\alpha\left(\lambda\right)}{TX_\lambda}\bar{n}_\lambda\left(\bar{n}_\lambda+1\right), \end{aligned} \tag{16}$$

where (when only three phonon scattering is included)

$$X_\lambda\equiv\sum_{\lambda'}\sum_{\lambda''}\left(\Gamma^{\lambda''}_{\lambda\lambda'}+\Gamma^{\lambda'\lambda''}_{\lambda}\right). \tag{17}$$

In Eqs. 16 and 17, $\Gamma^{\lambda'\lambda''}_\lambda$ is the transition probability for processes in which a phonon λ vanishes and two phonons λ',λ'' are created. Accordingly, $\Gamma^{\lambda''}_{\lambda\lambda'}$ is the transition probability for the opposite process. The transition probabilities $\Gamma^{\lambda''}_{\lambda\lambda'},\Gamma^{\lambda'\lambda''}_{\lambda}$ can be obtained, for instance, from the golden rule or from the phonon self energy[41,42]. For example, one may write (here $\beta=1/k_BT$)

$$\begin{aligned} \sum_{\lambda'}\sum_{\lambda''}\Gamma^{\lambda'\lambda''}_\lambda=&18\frac{\beta\pi}{\hbar}\sum_{\lambda'}\sum_{\lambda''}\left|V\left(\lambda;\lambda';\lambda''\right)\right|^2 \\ &\times\left(\bar{n}_{\lambda'}+\bar{n}_{\lambda''}+1\right)\delta\left[\omega_\lambda-\omega_{\lambda'}-\omega_{\lambda''}\right], \end{aligned} \tag{18}$$

and in a similar way for the transition rates $\Gamma^{\lambda''}_{\lambda\lambda'}$ [41,42]. In Eq. 18, the coefficients $|V(\lambda;\lambda';\lambda'')|^2$ are given by Eq. 5. By Eq. 5, the decrease of the mass of the atoms $\kappa, \kappa', \kappa''$ relative to the third-order IFCs $\Phi_{\alpha\alpha'\alpha''}(0\kappa; l'\kappa'; \ldots; l''\kappa'')$ results in larger transition rates and shorter relaxation times (RT) in general. Also, the decrease of the phonon eigenvalues $\omega_\lambda, \omega_{\lambda'}, \omega_{\lambda''}$ has the same effect when other factors are fixed. These effects within the studied structures are considered in Sec. III B. The quantity $F_{\alpha,\lambda}$ is related to the RT as[40]

$$\tau_\alpha(\lambda) = \frac{TF_{\alpha,\lambda}}{\hbar\omega_\lambda v_\alpha(\lambda)}, \tag{19}$$

thus Eq. 15 can be written as

$$\kappa_{\alpha\beta} = \frac{1}{V}\sum_\lambda v_\alpha(\lambda)\, v_\beta(\lambda)\, c_v(\lambda)\, \tau_\beta(\lambda), \tag{20}$$

where the heat capacity at constant volume for the phonon state λ may be written as

$$c_v(\lambda) = k_B\beta^2\hbar^2\omega_\lambda^2\bar{n}_\lambda(\bar{n}_\lambda + 1). \tag{21}$$

The shortcomings of the method used to calculate the lattice thermal conductivity in this work are discussed in Ref.[34]. Recently, computational studies for real materials, where the temperature dependence of the IFCs is taken into account have been carried out[43,44]. This effect is neglected in the present approach and it may have some significance on the present results.

C. Studied structures and computational details

The space group of all the studied structures is $I\bar{4}3m$ (217). The silicon clathrate framework Si_{23} has 23 atoms in the primitive unit cell, while the Zintl clathrates $[Si_{19}P_4]Cl_4$ and $Na_4[Al_4Si_{19}]$ have 27 atoms in the primitive unit cell. The crystallographic body-centered cubic unit cell of $[Si_{19}P_4]Cl_4$ and $Na_4[Al_4Si_{19}]$ with 54 atoms is illustrated in Fig. 1. The parent silicon framework can be considered to be composed of fused polyhedral cages (cavities), where the vertices correspond to four-coordinated silicon atoms. The framework heteroatoms Al/P occupy the 8c Wyckoff position within the Si framework, while the Na/Cl guest atoms are located inside the polyhedral cages (Wyckoff position 8c)[6]. The $Na_4[Al_4Si_{19}]$ and $[Si_{19}P_4]Cl_4$ structures can be classified as anionic and cationic clathrates, respectively[46]. In the so-called anionic Zintl clathrates such as Na4[Al4Si19], there is a charge transfer from the less electronegative guest atoms (Na) to the framework atoms (Si-Al). In the so-called cationic Zintl clathrates such as [Si19P4]Cl4, there is a charge transfer from the less electronegative framework atoms (Si-P) to the guest atoms (Cl). The bonding within the framework can be considered to be covalent, while the framework-guest interactions are of ionic nature[47].

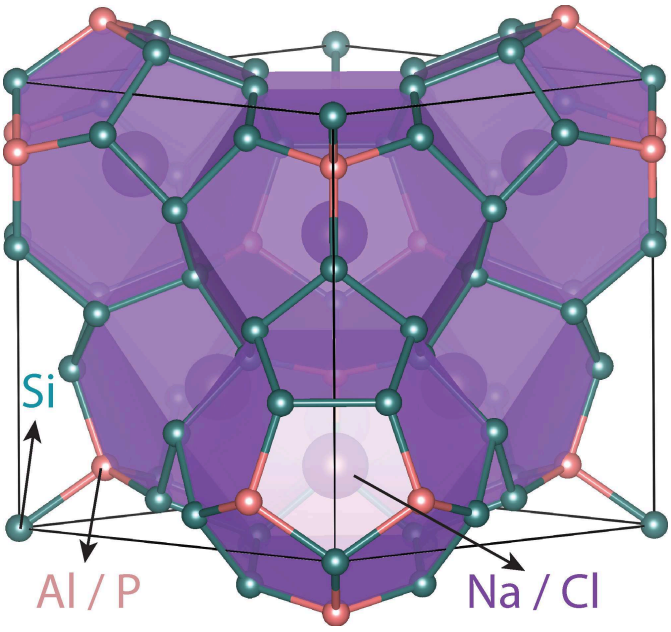

FIG. 1. The crystallographic body-centered cubic unit cell of the Zintl clathrates $[Si_{19}P_4]Cl_4$ and $Na_4[Al_4Si_{19}]$. The figure was prepared using the VESTA visualization program[45]. (Color online)

The *ab initio* density functional calculations to optimize the crystal structures and to calculate the phonon eigenvalues and eigenvectors were carried out with the Quantum Espresso program package (QE, version 5.0.3).[48] Atoms were described using ultrasoft pseudopotentials and plane wave basis set[49]. The Generalized Gradient Approximation (GGA) was applied by using the PBE exchange-correlation energy functionals[50]. If not otherwise mentioned, the applied computational parameters and methods were similar to those used in Ref.[34]. The results for the clathrate framework Si_{23}, used here for comparative analysis of the Zintl clathrates, were taken from Ref.[34]. A (6,6,6) mesh was used for the electronic **k** sampling, while the **q** meshes used phonon and lattice thermal conductivity calculations were (4,4,4) and (10,10,10), respectively. Both the lattice constants and the atomic positions of the studied structures were optimized by forcing the space group $I\bar{4}3m$. The optimized lattice constants were 10.10 Å, 10.00 Å, and 10.37 Å for Si_{23}, $[Si_{19}P_4]Cl_4$, and $Na_4[Al_4Si_{19}]$, respectively. The non-analytic corrections to dynamical matrices in the limit $\mathbf{q} \to 0$ were taken into account in the QE and ShengBTE calculations. The version 1.0.2 of ShengBTE was used. In the lattice thermal conductivity calculations, three-phonon and isotopic scattering were included. The constant scalebroad was set to 0.5 in all ShengBTE calculations[41,51]. For all structures, third-order IFCs were calculated up to 6th-nearest neigbours using the program thirdorder.py included in the ShengBTE distribution[52]. A $(3,3,3)$ supercell was used to calculate the third-order IFCs with thirdorder.py in

all cases.

The validity of the present computational approach was assessed in Ref.[34], for instance, by comparing the calculated lattice thermal conductivity values to the experimental ones in the case of the silicon diamond structure (d-Si). The difference between the calculated and experimental values was about 4%-13% within the temperature range 125-300 K, the smallest differences being obtained at higher temperatures.

III. RESULTS AND DISCUSSION

A. Phonon spectrum

The calculated phonon eigenvalues (dispersion relations) along high symmetry paths for the structures Si_{23}, $[Si_{19}P_4]Cl_4$ and $Na_4[Al_4Si_{19}]$ are shown in Fig. 2. The phonon dispersions are rather similar for all structures within the frequency range 200-500 cm^{-1}. For frequencies below 100 cm^{-1}, Si_{23} and $[Si_{19}P_4]Cl_4$ show rather similar spectrum while the spectrum for $Na_4[Al_4Si_{19}]$ appears to be different. The differences between Si_{23} and $[Si_{19}P_4]Cl_4$ are mostly due to the Cl guest atoms within the frequency range 100-200 cm^{-1} (this can be seen from the atom projected phonon density of states considered later in this section). The maximum frequencies of acoustic modes for $Na_4[Al_4Si_{19}]$ are about two times smaller than the corresponding values in the case of Si_{23} and $[Si_{19}P_4]Cl_4$. Furthermore, the acoustic and lowest-energy optical modes of the structure $Na_4[Al_4Si_{19}]$ show oscillatory behaviour, for example, along the high symmetry paths $\Gamma - P$ and $\Gamma - PA$, while in the case of Si_{23} and $[Si_{19}P_4]Cl_4$ this behaviour seems to be absent.

According to Eqs. 10 and 12 and since both structures with guest atoms have the same exponential factors, $e^{-i\mathbf{q}\cdot\mathbf{x}(l)}$, difference of the dynamical matrix elements $\{D_{\alpha\beta}(\kappa\kappa'|\mathbf{q})\}$ is due to the second-order IFCs divided by the atomic masses $D_{\alpha\beta}(l\kappa;0\kappa') = \Phi_{\alpha\beta}(l\kappa;0\kappa')/\sqrt{M_\kappa M_{\kappa'}}$ (Eq. 11). After one fixes the dynamical matrix, the eigenvectors can be calculated numerically: this and the preceding in mind one may infer that the differences in the dispersion relations for frequencies below 100 cm^{-1} indicate differences in $\{D_{\alpha\beta}(l\kappa;0\kappa')\}$ between the considered structures.

In Fig. 3, the so-called atom projected density of states $\rho_\kappa(\omega) = 1/N\sum_\lambda |\mathbf{e}(\kappa|\lambda)|^2 \delta(\omega-\omega_\lambda)$ and the participation ratio (PR) defined as[25,27,53,54]

$$PR = \frac{\left[\sum_\kappa |\mathbf{e}(\kappa|\lambda)|^2 M_\kappa^{-1}\right]^2}{N_a \sum_\kappa |\mathbf{e}(\kappa|\lambda)|^4 M_\kappa^{-2}}, \qquad (22)$$

are shown to further analyze the differences in the phonon spectrum of the studied structures. N_a is the number of atoms within the unit cell. If one considers $|\mathbf{e}(\kappa|\lambda)|^2$ as the probability distribution (Sec. II A), then $\rho_\kappa(\omega)$ may be considered as the expected value of the phonon density of states (PDOS) for each κ. It can be seen from Fig. 3, that the contribution of the framework heteroatoms (Al and P) to $\rho_\kappa(\omega)$ is rather similar to that of the Si framework atoms, when comparing all three structures. However, some differences can be identified, for instance, at the frequencies 3-6 THz. The guest atoms Cl and Na mainly contribute to the phonon modes at the frequencies below 5 THz. Further, for $Na_4[Al_4Si_{19}]$, there is a relatively large contribution of Na guest atoms at 2 THz, while an analogous contribution from the Cl guest atoms is absent in the case of $[Si_{19}P_4]Cl_4$.

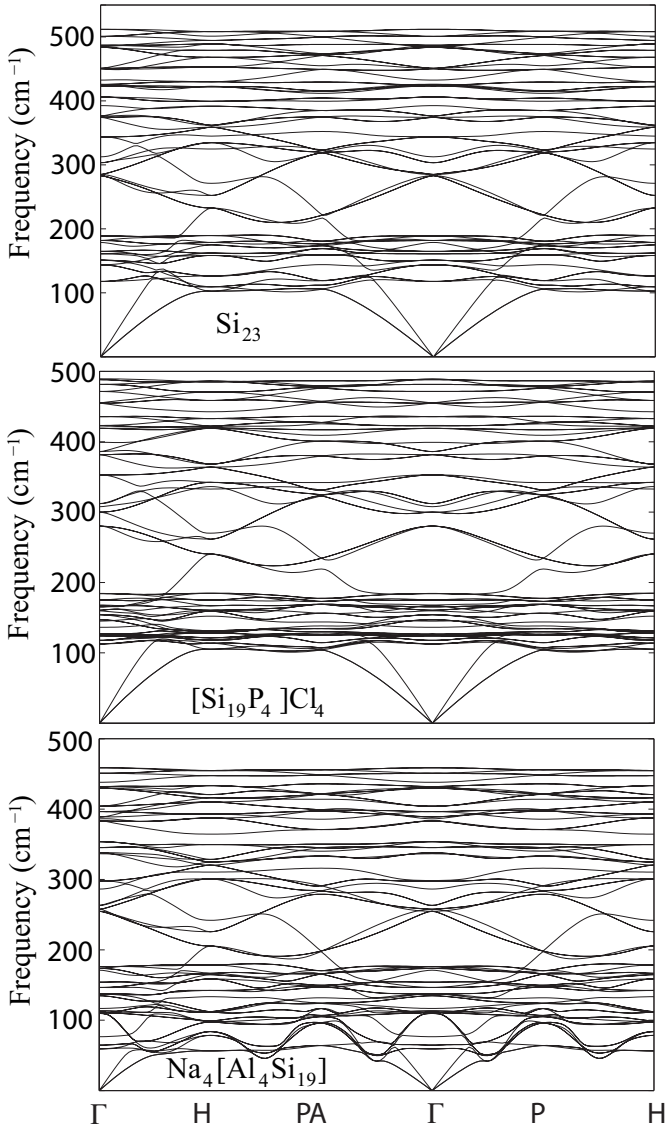

FIG. 2. Phonon eigenvalues as a function of wave vector (dispersion relations) along high symmetry paths in the first Brillouin zone for Si_{23}, $[Si_{19}P_4]Cl_4$ and $Na_4[Al_4Si_{19}]$.

The PR can be used to study the localization of the phonon modes[53]. The modes with rather local characteristics are expected to have the PR values near N_a^{-1} (only few atoms are displaced in the mode), while the PR values of about 1 indicate the opposite. In Si_{23} and

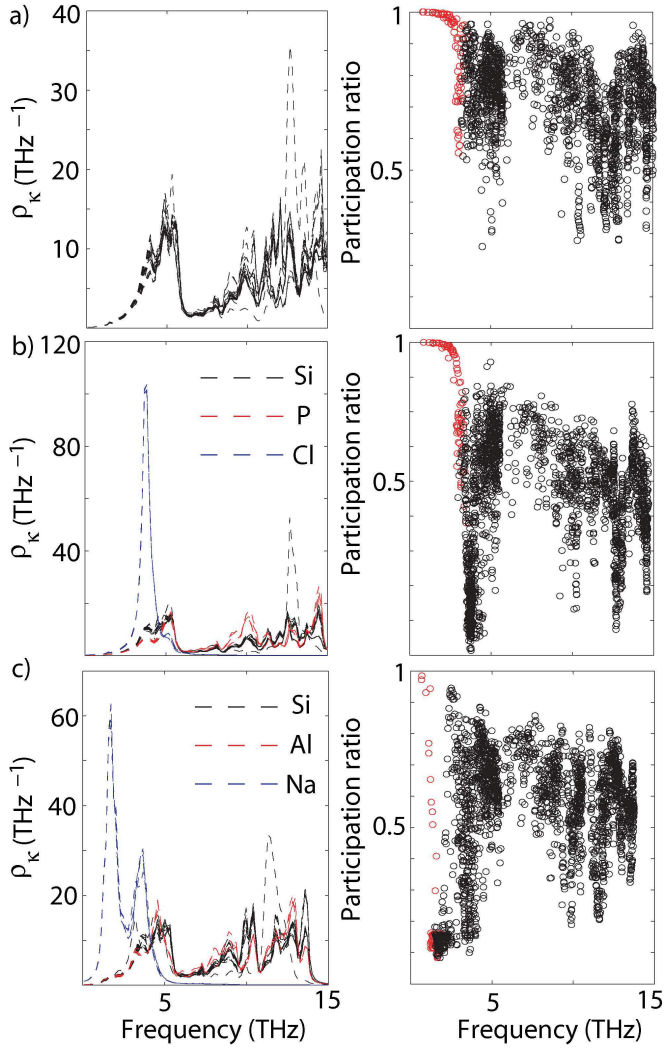

FIG. 3. The atom projected density of states $\rho_\kappa(\omega)$ and participation ratio for each structure. (a) Si_{23}, (b) $[Si_{19}P_4]Cl_4$ and (c) $Na_4[Al_4Si_{19}]$. The participation ratio values for the acoustic modes are drawn in red. (Color online)

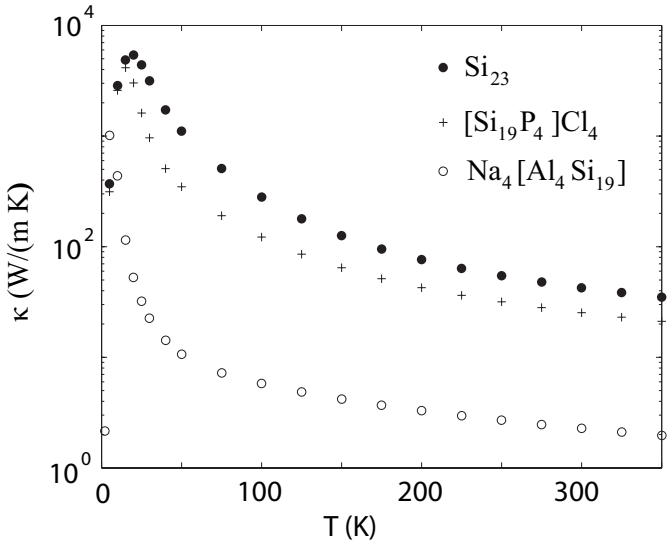

FIG. 4. The calculated lattice thermal conductivity values for the structures Si_{23}, $[Si_{19}P_4]Cl_4$ and $Na_4[Al_4Si_{19}]$.

$[Si_{19}P_4]Cl_4$, the PR values for the acoustic modes are approximately between 1 and 0.5, while for $Na_4[Al_4Si_{19}]$ PR values as low as 0.1 are obtained and most of the PR values for the acoustic modes are clustered between 0.1 and 0.2. This indicates that the acoustic modes of $Na_4[Al_4Si_{19}]$ seem to have more local characteristics than the acoustic modes in the other two structures.

To estimate the difference in the harmonic interactions, the following mean values for the second-order IFCs are used

$$D(\kappa) \equiv \frac{1}{9N_a} \sum_{\alpha,\beta,\kappa'} |D_{\alpha\beta}(0\kappa; 0\kappa')| . \qquad (23)$$

The values $D(\kappa)$ on average for the Na guest atoms are about 25% smaller than those for the Cl guest atoms. Also, the Al framework heteroatoms atoms show approximately 21% smaller $D(\kappa)$ values on average than obtained for the P heteroatoms. Further, the Si framework atoms have about 10% smaller $D(\kappa)$ values on average in the structures $[Si_{19}P_4]Cl_4$ and $Na_4[Al_4Si_{19}]$ in comparison to the framework heteroatoms P and Al. Lastly, the Na and Cl guest atoms have approximately five times smaller $D(\kappa)$ values on average than obtained for the framework atoms, that is, the ratio is almost the same in both cases.

To summarize, the framework heteroatoms and the Si framework atoms seem to have rather similar effect on the phonon spectrum in all the studied structures. Furthermore, the Na and Cl guest atoms appear to have a rather large effect on the phonon spectrum at the frequencies below 5 THz and Na guest atoms seem to flatten the acoustic phonon dispersion relations in a more distinct manner in comparison to the Cl guest atoms.

B. Results for lattice thermal conductivity and related quantities

The calculated thermal conductivity values as a function of temperature for all studied structures are shown in Fig. 4. The lattice thermal conductivities for Si_{23} and $[Si_{19}P_4]Cl_4$ within the temperature range 100-300 K are 282-43 W/(m K) and 122-25 W/(m K), respectively. Within the same temperature range, the lattice thermal conductivities for $Na_4[Al_4Si_{19}]$ are approximately 6-2 W/(m K). Thus, the present results indicate that $Na_4[Al_4Si_{19}]$ has about twenty times smaller lattice thermal conductivity values in comparison to Si_{23} and about ten times smaller values in comparison to $[Si_{19}P_4]Cl_4$. In Refs.[29,30], about three times smaller lattice thermal conductivity at 300 K were obtained for Si_{23} (or Si_{46}-VIII) by using more approximate models for the lattice conductivity based on the linearized BTE than used in

the present work. Further, about four times lower lattice thermal conductivity at 300 K were obtained for the clathrates $Ba_8Al_{16}Si_{30}$ and $Ba_8Cu_6Si_{40}$ in Ref.[30], than obtained here for $Na_4[Al_4Si_{19}]$.

The lattice thermal conductivity values for each state λ in conjunction with the RTs $\tau(\lambda)$, phonon phase space $P_3(\lambda)$, and quantities $\xi(\lambda)$ are shown in Fig. 5. For $Na_4[Al_4Si_{19}]$, the largest lattice thermal conductivity contributions of acoustic modes are rather systematically smaller than in the case of Si_{23} or $[Si_{19}P_4]Cl_4$. A similar difference can be seen between the structures Si_{23} and $[Si_{19}P_4]Cl_4$. Si_{23} and $[Si_{19}P_4]Cl_4$ show rather similar values for the quantity $\xi(\lambda)$. As in the case of lattice thermal conductivity, $Na_4[Al_4Si_{19}]$ also has a rather different different distribution of values of the quantity $\xi(\lambda)$, the values for acoustic modes being mostly smaller in comparison to Si_{23} or $[Si_{19}P_4]Cl_4$. This is not that surprising as such because the harmonic phonon spectrum for the acoustic modes of $Na_4[Al_4Si_{19}]$ is rather different in comparison to the other two structures (Fig. 2). The flattening of the acoustic modes as a function of $\mathbf{q}$ has ($\omega(\lambda)$ have smaller values for acoustic modes), for example, the following effects on $\xi(\lambda)$ at fixed temperature T_0: smaller values of $\omega(\lambda)$ increase $\bar{n}_\lambda$ and thus $c_v(\lambda)$. The flattening decreases the group velocity $\mathbf{v}(\lambda)$, thus the flattening has opposite effect on $\mathbf{v}(\lambda)$ and $c_v(\lambda)$. In the case of $Na_4[Al_4Si_{19}]$, the change in the harmonic phonon spectrum seems to favor the reduced group velocities more than the increase of $c_v(\lambda)$, resulting in the smaller values of $\xi(\lambda)$ for acoustic modes.

The RTs, shown in Fig. 5, reveal some differences between Si_{23} and $[Si_{19}P_4]Cl_4$, the former having larger maximum values of $\tau(\lambda)$, in particular for acoustic modes. This seems to be the main reason for the different values of lattice thermal conductivity obtained for $[Si_{19}P_4]Cl_4$ and Si_{23}. The RTs for $Na_4[Al_4Si_{19}]$ are in general smaller than obtained for $[Si_{19}P_4]Cl_4$ and Si_{23}. Compared with $[Si_{19}P_4]Cl_4$, the maximum values for the acoustic modes of $Na_4[Al_4Si_{19}]$ are about ten times smaller. For $[Si_{19}P_4]Cl_4$ and $Na_4[Al_4Si_{19}]$, it appears that the third-order coefficients $V(\lambda;\lambda';\lambda'')$ may have larger values than in the case of Si_{23}.

The distribution of phonon phase space values $P_3(\lambda) \propto \tau^{-1}(\lambda)$, also shown in Fig. 5, are rather different for all structures despite the rather similar phonon spectra for the structures Si_{23} and $[Si_{19}P_4]Cl_4$. The maximum values are, perhaps surprisingly, largest for Si_{23}. For example, Si_{23} has larger $P_3(\lambda)$ values for acoustic modes than d-Si[34], which probably is one of the reasons behing the smaller lattice thermal conductivity of Si_{23} in comparison to d-Si. The maximum values of $P_3(\lambda)$ are rather similar for $[Si_{19}P_4]Cl_4$ and $Na_4[Al_4Si_{19}]$. However, for $Na_4[Al_4Si_{19}]$, the P_3 values for acoustic modes are more clustered than for the other structures and there are practically no values below 0.6, while for other structures there are rather many states with values smaller than this. Thus, it seems that the P_3 values are one the reasons behind the smaller RTs obtained for $Na_4[Al_4Si_{19}]$.

In Fig. 6, the third-order IFCs as a function of distance are shown. The following quantities are used in Fig. 6

$$\begin{aligned} &d(0\kappa_1; l_2\kappa_2; l_3\kappa_3) \\ &\equiv |x(\kappa_1) - x(l_2\kappa_2)| + |x(\kappa_1) - x(l_3\kappa_3)|, \end{aligned} \quad (24)$$

$$\Phi_3 \equiv \frac{1}{27} \sum_{\alpha_1,\alpha_2,\alpha_3} |\Phi_{\alpha_1\alpha_2\alpha_3}(0\kappa_1; l_2\kappa_2; l_3\kappa_3)|. \quad (25)$$

As can be seen, the third-order IFCs of the three studied structures do not show such large differences that could have been expected based on the differences in the calculated RTs. Therefore, it seems that the different RTs are mostly due to the harmonic quantities included in the anharmonic Hamiltonian and some possible reasons for the different RTs of $Na_4[Al_4Si_{19}]$ are discussed next. As mentioned in Sec. II B, the decrease of mass of the atoms and the term $\omega_\lambda\omega_{\lambda'}\omega_{\lambda'}$ in general decreases the value of the RTs. Also, as $\omega_{\lambda'}$ and $\omega_{\lambda''}$ have smaller values, the following term $(\bar{n}_{\lambda'} + \bar{n}_{\lambda''} + 1)$ in Eq. 18 further decreases the value of the RTs. Since the PR values for the acoustic modes in the case of $Na_4[Al_4Si_{19}]$ are rather small (only few atoms vibrate in a particular state), the probabilities $|\mathbf{e}(\kappa|\lambda)|^2$ and thus the phonon eigenvectors $\mathbf{e}(\kappa|\lambda)$ for the acoustic modes are expected to be rather large, which in turn decreases the RTs of these modes through the coefficients $|V(\lambda;\lambda';\lambda'')|^2$. The exponential factors, $e^{i\mathbf{q}_i\cdot\mathbf{x}(l_i)}$, are identical in all structures. Together with the differing P_3 and smaller group velocity values of the acoustic modes, these mentioned factors may have some significance in explaining the smaller RT and lattice thermal conductivity values of $Na_4[Al_4Si_{19}]$. To summarize, the stronger anharmonicity of the structure $Na_4[Al_4Si_{19}]$ in comparison to Si_{23} and $[Si_{19}P_4]Cl_4$ seems to arise mostly from the differing harmonic quantities instead of the third-order IFCs.

One way to measure the anharmonicity of a structure are the so-called Grüneisen parameters. By using the perturbation theory, it has been shown that the Grüneisen parameters can be written as[55]

$$\begin{aligned} \gamma_{\mu\nu}(\lambda) =& -\sum_{j'=4}^{3n} \frac{12V_{\mu\nu}(0j')V(0j';\lambda;-\lambda)}{\hbar^2\omega_{0j'}\omega_\lambda} \\ &-\frac{2V_{\mu\nu}(\lambda;-\lambda)}{\hbar\omega_\lambda}, \end{aligned} \quad (26)$$

where the first term on the right hand side vanishes if the position of every atom in the unit cell is determined by the symmetry (no internal strain). In Eq. 26, the coefficients like $V(\lambda;\lambda';\lambda'')$ are given by Eq. 5 and

$$\begin{aligned} V_{\mu\nu}(\lambda;\lambda') =& \frac{\hbar}{4} \sum_{\kappa,\alpha} \sum_{l',\kappa',\alpha'} \sum_{l'',\kappa''} \Phi_{\alpha\alpha'\mu}(0\kappa; l'\kappa'; l''\kappa'') \\ &\times \frac{e_\alpha(\kappa|\lambda)\, e_{\alpha'}(\kappa'|\lambda')}{\sqrt{M_\kappa M_{\kappa'}\omega_\lambda\omega_{\lambda'}}} e^{i\mathbf{q}'\cdot\mathbf{x}(l')} x_\nu(l''\kappa''). \end{aligned} \quad (27)$$

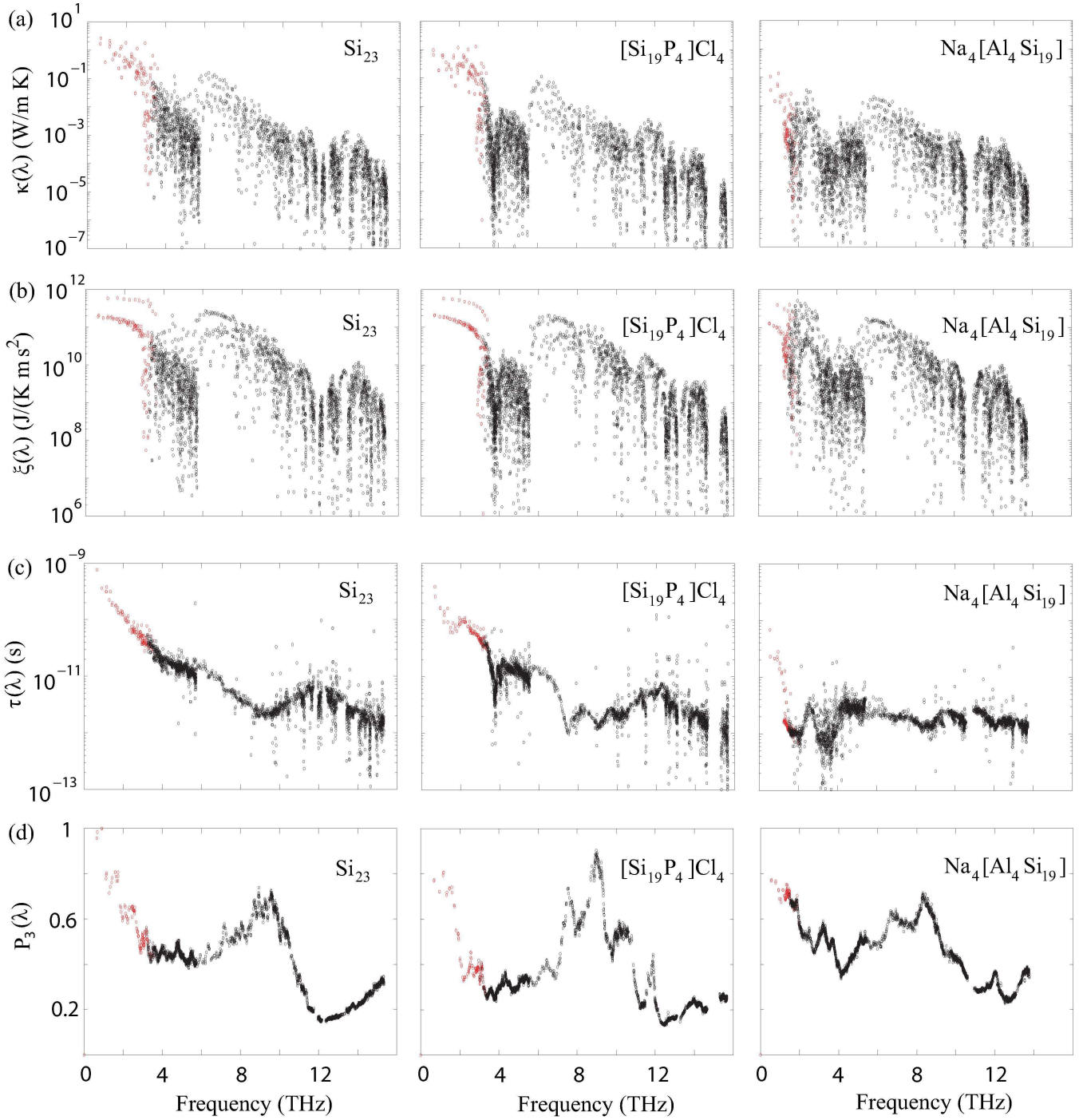

FIG. 5. The calculated values for each state λ as a function of phonon frequency for the structures Si_{23}, $[Si_{19}P_4]Cl_4$ and $Na_4[Al_4Si_{19}]$ at 300 K. (a) The lattice thermal conductivity $\kappa(\lambda) = 1/3\sum_\alpha \kappa_{\alpha\alpha}(\lambda)$ (negative values are not shown), (b) quantities $\xi(\lambda) \equiv 1/(3V)\sum_\alpha v_\alpha^2(\lambda)\, c_v(\lambda)$, (c) relaxation times $\tau(\lambda) \equiv 1/3\sum_\alpha \tau_\alpha(\lambda)$ (negative values are not shown) and (d) phonon phase space $P_3(\lambda)$. For all quantities, the acoustic modes are drawn in red and the optical modes in black. The reported $P_3(\lambda)$ values are unitless relative values obtained from $P_3(\lambda) / \max\left\{ P_3(\lambda)|_{Si_{23}} \right\}$. (Color online)

The Grüneisen parameters can also be written as

$$\gamma_{\mu\nu}(\lambda) = -\frac{1}{\omega_\lambda}\frac{\partial \omega_\lambda}{\partial \eta_{\mu\nu}}, \tag{28}$$

and furthermore, in the case of cubic crystals

$$\frac{1}{3}\gamma_{\mu\mu}(\lambda) = -\frac{V}{\omega_\lambda}\frac{\partial \omega_\lambda}{\partial V} \equiv \gamma(\lambda). \tag{29}$$

When the phonon-phonon interaction is approximated in

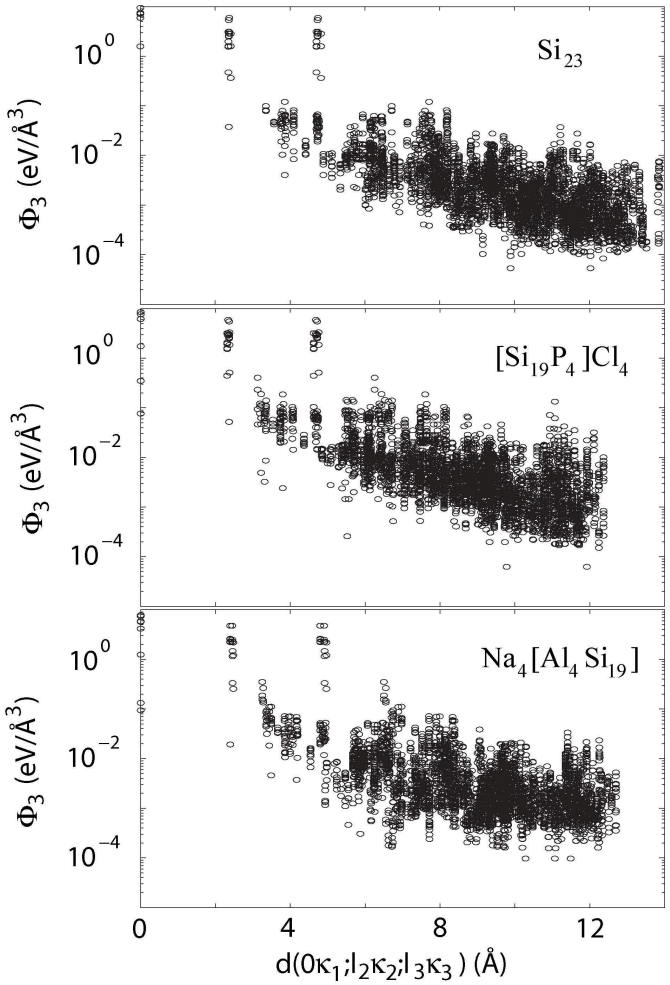

FIG. 6. The calculated third-order IFCs for Si_{23}, $[Si_{19}P_4]Cl_4$ and $Na_4[Al_4Si_{19}]$. Here, $d\,(0\kappa_1; l_2\kappa_2; l_3\kappa_3)$ and Φ_3 are given by Eqs. 24 and 25.

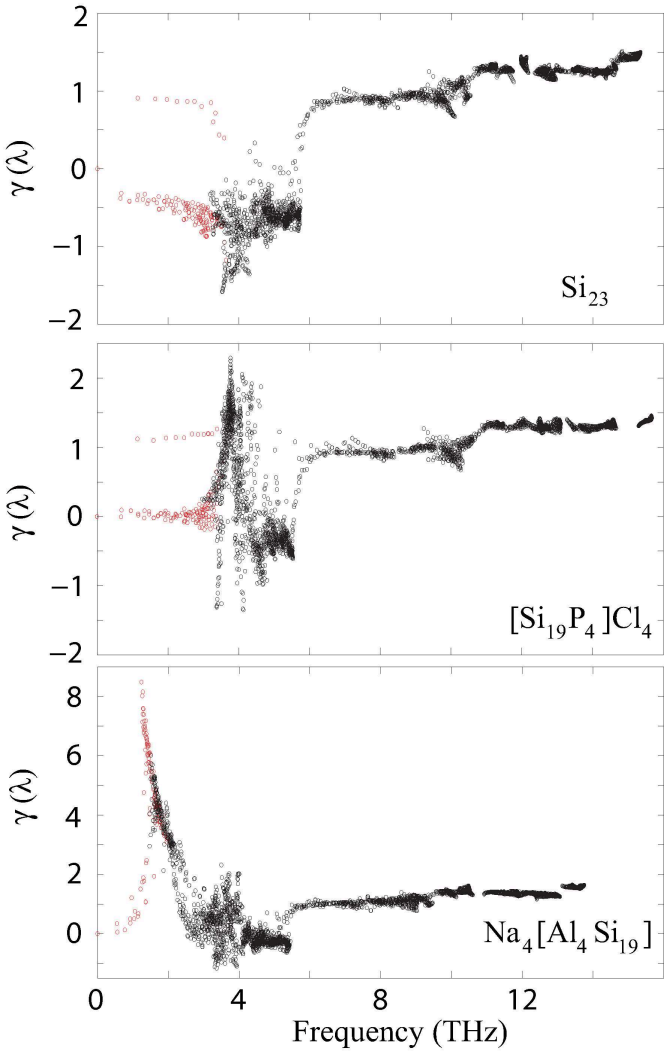

FIG. 7. The calculated Grüneisen parameter values for Si_{23}, $[Si_{19}P_4]Cl_4$ and $Na_4[Al_4Si_{19}]$. The acoustic modes are shown in red and the optical modes in black. (Color online)

the so-called continuum theory, it has been shown that the square of the (averaged) Grüneisen parameter is inversely proportional to the mean free path and thus the lifetime of phonons[36].

The Grüneisen parameters are sometimes used for calculating the thermal expansion of materials. There is some evidence that, for instance, crystalline materials which have negative thermal expansion (NTE) over rather wide temperature ranges can have relatively low lattice thermal conductivity values[56,57] (measured for polycrystalline samples, however). This behaviour of NTE materials would be rather logical since, as mentioned, in the continuum theory $\tau \propto \gamma^{-2}$ (τ and γ are some average values) and within the so-called quasiharmonic approximation (QHA), the coefficient of thermal expansion (CTE) can be written as (see for example Refs.[58]) $\alpha_{\mu_1\nu_1} = \sum_{\mu_2,\nu_2} \sum_{\lambda} s^T_{\mu_1\nu_1\mu_2\nu_2} c_v\,(\lambda)\,\gamma_{\mu_1\nu_1}\,(\lambda)$, where $s^T_{\mu_1\nu_1\mu_2\nu_2}$ is the isothermal second-order compliance tensor, inverse to the isothermal second-order elastic constant $c^T_{\mu_1\nu_1\mu_2\nu_2}$. That is, the $\gamma_{\mu\nu}\,(\lambda)$ are usually expected to have relatively large absolute values for materials which have rather large absolute value of the CTE. There is some evidence that the silicon clathrate framework VII possesses rather unusual NTE behavior, while Si_{23} (or VIII), for instance, has CTE that is rather similar to d-Si[59].

The calculated Grüneisen parameter values $\gamma\,(\lambda)$ as a function of frequency for each structure are shown in Fig. 7. For acoustic modes, the distribution of $\gamma\,(\lambda)$ values in the case of Si_{23} and $[Si_{19}P_4]Cl_4$ is rather similar, while for $Na_4[Al_4Si_{19}]$ fairly different result is obtained. Compared with $Na_4[Al_4Si_{19}]$, the maximum values of $\gamma\,(\lambda)$ are about eight times smaller in the case of Si_{23} and $[Si_{19}P_4]Cl_4$. For $Na_4[Al_4Si_{19}]$, the lowest-energy optical modes have about three times larger Grüneisen parameter values in comparison to $[Si_{19}P_4]Cl_4$. For Si_{23}, the Grüneisen parameter results are similar to those obtained in Refs.[59] and[29].

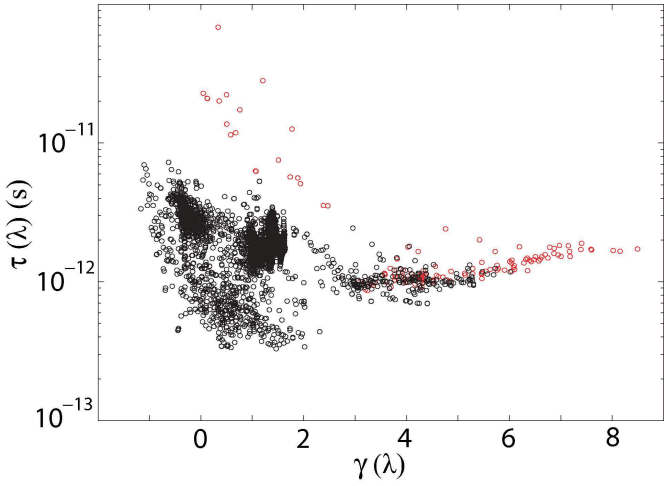

FIG. 8. The calculated RTs and the corresponding Grüneisen parameter values for each state λ in $Na_4[Al_4Si_{19}]$. The acoustic modes are shown in red and the optical modes in black. (Color online)

To study the relationship between the RTs and Grüneisen parameters, these quantities are depicted in Fig. 8 for $Na_4[Al_4Si_{19}]$. For the acoustic modes, when $\gamma\,(\lambda) \geq 2$, the maximum $\tau\,(\lambda)$ values are approximately 2×10^{-12} s, which is about one order of magnitude smaller than the largest values obtained. Thus, these modes have a rather small contribution to the lattice thermal conductivity. The smallest $\tau\,(\lambda)$ values for the acoustic modes are obtained when the Grüneisen parameters have values between 3 and 4. The relationship shown in Fig. 8 indicates that in some cases, there can be a connection between the relatively large absolute values of CTE and rather low lattice thermal conductivities.

As already mentioned in Sec. I, several mechanisms have been proposed to explain the rather small lattice thermal conductivity of various Zintl clathrates. In Ref.[17], for instance, it was concluded for the $Ba_8Ga_{16}Ge_{30}$ clathrate based on inelastic neutron scattering data that the reduction of the lattice thermal conductivity is mostly due to the flattening of the phonon dispersion relations caused by the guest atoms instead the shorter RTs of the phonons. In Ref.[25], inelastic x-ray scattering and *ab initio* lattice dynamical studies on the Ba_8Si_{46} clathrate resulted in the conclusion that the reduction of the lattice thermal conductivity follows from the changes in the harmonic spectrum induced by the guest-framework interactions and that the reduced RTs have a rather small significance. In contrast, in an *ab initio* lattice dynamical study for the $Ba_8Ga_{16}Ge_{30}$ clathrate[27], the largest reduction in the lattice thermal conductivity was suggested to arise from the smaller RT values, while the reduction of the phonon group velocities was found to have a smaller effect (the BTE was not solved iteratively, but within the single-mode relaxation time approximation).

The present results show similarities with the results obtained in Ref.[27] for the $Ba_8Ga_{16}Ge_{30}$ clathrate and in Ref.[60] for the $YbFe_4Sb_{12}$ skutterudite. In the case of $YbFe_4Sb_{12}$,[60] it was summarized that the increased phonon scattering is due to the differing phonon phase space, third-order IFCs having rather marginal effect on the reduction of the lattice thermal conductivity. The results of the present work show that for materials with relatively similar third-order IFCs, there can be rather significant changes in anharmonicity and in the lattice thermal conductivity values, which essentially follow from the differing second-order IFCs. To sum up some central findings of the present work: in the case of $Na_4[Al_4Si_{19}]$, the second-order IFCs seem to produce the harmonic phonon spectrum such that three-phonon phase space favors the phonon scattering and the phonon eigenvectors $\mathbf{e}\,(\kappa|\lambda)$ have rather large values for phonons of smallest frequencies (localization). These effects facilitate the reduction of RTs and phonon group velocities, which in turn leads to the reduced lattice thermal conductivity values. The hypothetical structures studied here possess rather high symmetry (symmetry is forced in the calculation) and it is probable that possible structural disorder decreases the lattice thermal conductivity even further[61,62].

IV. CONCLUSIONS

The lattice thermal conductivity of the silicon clathrate framework Si_{23} and two Zintl clathrates, $[Si_{19}P_4]Cl_4$ and $Na_4[Al_4Si_{19}]$, was investigated by using *ab initio* lattice dynamics together with an iterative solution of the linearized BTE. The lattice thermal conductivity of the structure $Na_4[Al_4Si_{19}]$ was found to be about one order of magnitude lower at 300 K in comparison to the other two materials studied here. The lower lattice thermal conductivity of $Na_4[Al_4Si_{19}]$ is mostly due to lower relaxation times and phonon group velocities, which differ from Si_{23} and $[Si_{19}P_4]Cl_4$ largely due second-order IFCs. Furthermore, it appears that the anharmonicity of two similar crystalline materials can be rather different from one another mostly because of differing second-order IFCs. The present results may shed light on the understanding about the lattice thermal conductivity of clathrates and skutterudites, for example, which can give further guidance for the discovery of more efficient thermoelectric materials.

ACKNOWLEDGMENTS

We gratefully acknowledge funding from the Foundation for Research of Natural Resources in Finland (grant 17591/13). The computing resources for this work were provided by the Finnish Grid Infrastructure (FGI) and CSC - the Finnish IT Center for Science.

* ville.j.harkonen@jyu.fi
† antti.j.karttunen@iki.fi

[1] A. F. Ioffe, *Semiconductor Thermoelements and Thermoelectric Cooling* (Infosearch Limited London, 1957) pp. 1–184.
[2] G. A. Slack and D. Rowe, CRC, Boca Raton, FL , 407 (1995).
[3] J. S. Kasper, P. Hagenmuller, M. Pouchard, and C. Cros, Science **150**, 1713 (1965).
[4] G. Nolas, J. Cohn, G. Slack, and S. Schujman, Appl. Phys. Lett. **73**, 178 (1998).
[5] K. A. Kovnir and A. V. Shevelkov, Russ. Chem. Rev. **73**, 923 (2004).
[6] A. J. Karttunen, T. F. Fassler, M. Linnolahti, and T. A. Pakkanen, Inorg. Chem. **50**, 1733 (2010).
[7] T. Takabatake, K. Suekuni, T. Nakayama, and E. Kaneshita, Rev. Mod. Phys. **86**, 669 (2014).
[8] P. Norouzzadeh, C. W. Myles, and D. Vashaee, Sci. Rep. **4**, 7028 (2014).
[9] J. L. Cohn, G. S. Nolas, V. Fessatidis, T. H. Metcalf, and G. A. Slack, Phys. Rev. Lett. **82**, 779 (1999).
[10] J. S. Tse, K. Uehara, R. Rousseau, A. Ker, C. I. Ratcliffe, M. A. White, and G. MacKay, Phys. Rev. Lett. **85**, 114 (2000).
[11] J. Dong, O. F. Sankey, and C. W. Myles, Phys. Rev. Lett. **86**, 2361 (2001).
[12] G. Nolas, M. Beekman, J. Gryko, G. Lamberton Jr, T. Tritt, and P. McMillan, Appl. Phys. lett. **82**, 910 (2003).
[13] A. Bentien, M. Christensen, J. D. Bryan, A. Sanchez, S. Paschen, F. Steglich, G. D. Stucky, and B. B. Iversen, Phys. Rev. B **69**, 045107 (2004).
[14] M. A. Avila, K. Suekuni, K. Umeo, H. Fukuoka, S. Yamanaka, and T. Takabatake, Phys. Rev. B **74**, 125109 (2006).
[15] K. Suekuni, M. A. Avila, K. Umeo, and T. Takabatake, Phys. Rev. B **75**, 195210 (2007).
[16] Y. Takasu, T. Hasegawa, N. Ogita, M. Udagawa, M. A. Avila, K. Suekuni, and T. Takabatake, Phys. Rev. Lett. **100**, 165503 (2008).
[17] M. Christensen, A. B. Abrahamsen, N. B. Christensen, F. Juranyi, N. H. Andersen, K. Lefmann, J. Andreasson, C. R. Bahl, and B. B. Iversen, Nature Mater. **7**, 811 (2008).
[18] M. Avila, K. Suekuni, K. Umeo, H. Fukuoka, S. Yamanaka, and T. Takabatake, Appl. Phys. Lett. **92**, 041901 (2008).
[19] M. Christensen, S. Johnsen, F. Juranyi, and B. B. Iversen, J. Appl. Phys. **105**, 073508 (2009).
[20] M. Christensen, S. Johnsen, and B. B. Iversen, Dalton Trans. **39**, 978 (2010).
[21] C. Candolfi, U. Aydemir, A. Ormeci, W. Carrillo-Cabrera, U. Burkhardt, M. Baitinger, N. Oeschler, F. Steglich, and Y. Grin, J. Appl. Phys. **110**, 043715 (2011).
[22] H. Euchner, S. Pailhès, L. T. K. Nguyen, W. Assmus, F. Ritter, A. Haghighirad, Y. Grin, S. Paschen, and M. de Boissieu, Phys. Rev. B **86**, 224303 (2012).
[23] J. Fulmer, O. I. Lebedev, V. V. Roddatis, D. C. Kaseman, S. Sen, J.-A. Dolyniuk, K. Lee, A. V. Olenev, and K. Kovnir, J. Am. Chem. Soc. **135**, 12313 (2013).
[24] Y. He and G. Galli, Nano Lett. **14**, 2920 (2014).
[25] S. Pailhès, H. Euchner, V. M. Giordano, R. Debord, A. Assy, S. Gomès, A. Bosak, D. Machon, S. Paschen, and M. de Boissieu, Phys. Rev. Lett. **113**, 025506 (2014).
[26] R. Castillo, W. Schnelle, M. Bobnar, U. Burkhardt, B. Böhme, M. Baitinger, U. Schwarz, and Y. Grin, Z. Anorg. Allg. Chem. **641**, 206 (2015).
[27] T. Tadano, Y. Gohda, and S. Tsuneyuki, Phys. Rev. Lett. **114**, 095501 (2015).
[28] K. Kishimoto, S. Koda, K. Akai, and T. Koyanagi, J. Appl. Phys. **118**, 125103 (2015).
[29] P. Norouzzadeh and C. W. Myles, J. Mater. Sci. **51**, 4538 (2016).
[30] G. K. Madsen, A. Katre, and C. Bera, Phys. Status Solidi A **213**, 802 (2016).
[31] K. Huang and M. Born, *Dynamical Theory of Crystal Lattices* (Clarendon Press Oxford, 1954) pp. 293–306.
[32] A. Maradudin, E. Montroll, G. Weiss, and I. Ipatova, *Theory of The Lattice Dynamics in The Harmonic Approximation*, Vol. Supplement 3 (Academic Press, 1971) pp. 6–57.
[33] A. Maradudin and G. Horton, *Elements of The Theory of Lattice Dynamics*, Vol. 1 (Amsterdam: North-Holland, 1974) pp. 1–82.
[34] V. J. Härkönen and A. J. Karttunen, Phys. Rev. B **93**, 024307 (2016).
[35] V. J. Härkönen, arXiv preprint arXiv:1603.06376 (2016).
[36] J. M. Ziman, *Electrons and Phonons: The Theory of Transport Phenomena in Solids* (Oxford University Press, 1960) pp. 264–298.
[37] G. P. Srivastava, *The Physics of Phonons* (CRC Press, 1990) p. 122.
[38] M. Omini and A. Sparavigna, Physica B **212**, 101 (1995).
[39] M. Omini and A. Sparavigna, Phys. Rev. B **53**, 9064 (1996).
[40] A. Ward, D. A. Broido, D. A. Stewart, and G. Deinzer, Phys. Rev. B **80**, 125203 (2009).
[41] W. Li, J. Carrete, N. A. Katcho, and N. Mingo, Comput. Phys. Commun. **185**, 1747 (2014).
[42] A. Maradudin and A. Fein, Phys. Rev. **128**, 2589 (1962).
[43] L. Paulatto, I. Errea, M. Calandra, and F. Mauri, Phys. Rev. B **91**, 054304 (2015).
[44] A. H. Romero, E. K. U. Gross, M. J. Verstraete, and O. Hellman, Phys. Rev. B **91**, 214310 (2015).
[45] K. Momma and F. Izumi, J. Appl. Crystallogr. **44**, 1272 (2011).
[46] A. Shevelkov and K. Kovnir, Struct. Bond. **139**, 97 (2011).
[47] C. Gatti, L. Bertini, N. P. Blake, and B. B. Iversen, Chem. Eur. J. **9**, 4556 (2003).
[48] P. Giannozzi, S. Baroni, N. Bonini, M. Calandra, R. Car, C. Cavazzoni, D. Ceresoli, G. L. Chiarotti, M. Cococcioni, I. Dabo, A. Dal Corso, S. de Gironcoli, S. Fabris, G. Fratesi, R. Gebauer, U. Gerstmann, C. Gougoussis, A. Kokalj, M. Lazzeri, L. Martin-Samos, N. Marzari, F. Mauri, R. Mazzarello, S. Paolini, A. Pasquarello, L. Paulatto, C. Sbraccia, S. Scandolo, G. Sclauzero, A. P. Seitsonen, A. Smogunov, P. Umari, and R. M. Wentzcovitch, J. Phys.: Condens. Matter **21**, 395502 (2009).
[49] K. F. Garrity, J. W. Bennett, K. M. Rabe, and D. Vanderbilt, Comput. Mater. Sci. **81**, 446 (2014).
[50] J. P. Perdew, K. Burke, and M. Ernzerhof, Phys. Rev. Lett. **77**, 3865 (1996).

[51] W. Li, N. Mingo, L. Lindsay, D. A. Broido, D. A. Stewart, and N. A. Katcho, Phys. Rev. B **85**, 195436 (2012).
[52] W. Li, L. Lindsay, D. A. Broido, D. A. Stewart, and N. Mingo, Phys. Rev. B **86**, 174307 (2012).
[53] R. J. Bell, P. Dean, and D. C. Hibbins-Butler, J. Phys. C **3**, 2111 (1970).
[54] J. Hafner and M. Krajci, J. Phys.: Condens. Matter **5**, 2489 (1993).
[55] T. Barron, M. Klein, G. Horton, and A. Maradudin, *Perturbation Theory of Anharmonic Crystals*, Vol. 1 (Amsterdam: North-Holland, 1974) pp. 391–450.
[56] C. A. Kennedy and M. A. White, Solid State Commun. **134**, 271 (2005).
[57] C. A. Kennedy, M. A. White, A. P. Wilkinson, and T. Varga, Appl. Phys. Lett. **90**, 151906 (2007).
[58] D. Wallace, *Thermodynamics of Crystals* (John Wiley & Sons, New York, 1972).
[59] V. J. Härkönen and A. J. Karttunen, Phys. Rev. B **89**, 024305 (2014).
[60] W. Li and N. Mingo, Phys. Rev. B **91**, 144304 (2015).
[61] B. Chakoumakos, B. Sales, D. Mandrus, and G. Nolas, J. Alloys Compd. **296**, 80 (2000).
[62] B. Chakoumakos, B. Sales, and D. Mandrus, J. Alloys Compd. **322**, 127 (2001).